Inorganic Chemistry

Article

pubs.acs.org/IC

True Composition and Structure of Hexagonal "$YAlO_3$", Actually $Y_3Al_3O_8CO_3$

Jun Li,[†] Andrew E. Smith,[†] Peng Jiang,[†] Judith K. Stalick,[‡] Arthur W. Sleight,[†] and M. A. Subramanian*[,†]

[†]Department of Chemistry, Oregon State University, Corvallis, Oregon 97331, United States

[‡]NIST Center for Neutron Research, National Institute of Standards and Technology, 100 Bureau Drive, Gaithersburg, Maryland 20899, United States

Supporting Information

ABSTRACT: The discovery of a brilliant-blue color upon the introduction of Mn^{3+} to the trigonal-bipyramidal (TBP) sites in $YInO_3$ has led to a search for other hosts for Mn^{3+} in TBP coordination. An obvious choice would be $YAlO_3$. This compound, which has only been prepared through a citrate precursor route, has long been considered isostructural with $YInO_3$. However, Mn^{3+} substitutions into $YAlO_3$ have failed to produce a product with the anticipated color. We find that the hexagonal structure for $YAlO_3$ with Al in TBP coordination proposed in 1963 cannot be correct based on its unit cell dimensions and bond-valence sums. Our studies indicate instead that all, or nearly all, of the Al in this compound has a coordination number (CN) of 6. Upon heating in air, this compound transforms to $YAlO_3$, with the perovskite structure liberating CO_2. The compound long assumed to be a hexagonal form of $YAlO_3$ is actually an oxycarbonate with the ideal composition $Y_3Al_3O_8CO_3$. The structure of this compound has been characterized by powder neutron and X-ray diffraction data obtained as a function of temperature, magic-angle-spinning ^{27}Al NMR, Fourier transform infrared, and transmission electron microscopy. Refinement of neutron diffraction data indicates a composition of $Y_3Al_3O_8CO_3$. We find that the hexagonal structures of $YGaO_3$ and $YFeO_3$ from the citrate route are also stabilized by small amounts of carbonate. Surprisingly, $Y_3Al_3O_8CO_3$ forms a complete solid solution with YBO_3 having tetrahedral borate groups. Other unlikely solid solutions were prepared in the $YAlO_3$–$YMnO_3$, $YAlO_3$–$YFeO_3$, $YAlO_3$–YBO_3, YBO_3–$YMnO_3$, YBO_3–$YFeO_3$, and YBO_3–$YGaO_3$ systems.

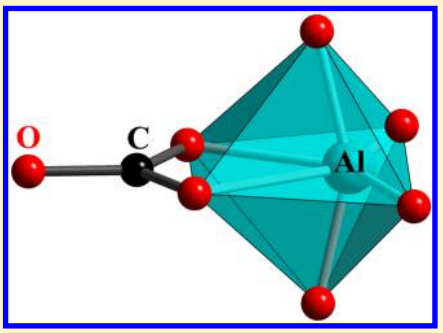

INTRODUCTION

Sheets of edge-shared octahedra form the basis for a rich variety of interesting structures. Such sheets have a composition of MO_2 and ideally have hexagonal symmetry (Figure 1). The strong electrostatic repulsion of M cations across the shared edges distorts the octahedra so that faces perpendicular to the *c* axis are significantly larger than other faces. Thus, the MO_3 polyhedra are actually trigonal antiprisms. Many MAO_2 compounds with these MO_2 layers are known. The A cations between the octahedral sheets can occupy octahedral, tetrahedral, trigonal-prismatic, or 2-fold linear sites in compounds with the delafossite structure, such as $AlCuO_2$.[1−4] The addition of O between the MO_2 sheets along with A cations leads to MAO_3 compounds, where the A cation can take a trigonal-bipyramidal (TBP) coordination as in $YMnO_3$ or a tetrahedral coordination as in YBO_3. Thus, two cation coordinations rare in oxides, TBP and 2-fold linear, are found in this family of MAO_{2-3} oxides. Intermediate O content phases can be prepared by O intercalation of MAO_2 phases (e.g., $CuScO_{2+x}$) or O deintercalation of MAO_3 phases (e.g., Y_2CuTiO_{6-x}).[4,5]

The hexagonal MAO_3 structures with the A cation in TBP coordination (Figure 1) have been reported for compounds where the M cation is a rare earth and the A cation can be In, Mn, Ga, Fe, or Al. Only for A = In and Mn does the reaction of Y_2O_3 plus A_2O_3 lead to the hexagonal phase when heating at the usual synthesis temperatures. The citrate route is required when A is Al or Fe. The hexagonal $YAlO_3$-type structure has also been reported for $RGaO_3$ (R = La, Pr, Nd, and Sm) compounds prepared by the citrate route.[6] The hexagonal form of $RGaO_3$ (R = Y, Ho, and Er) was subsequently prepared by quenching from a temperature higher than 1950 °C or by the precursor approach used to prepare hexagonal $YFeO_3$ and "$YAlO_3$".[7,8] Our attempts to prepare hexagonal $YGaO_3$ from Y_2O_3 plus Ga_2O_3 at temperatures up to 1600 °C failed. There are also $InAO_3$ compounds with this hexagonal structure, where In is now the M cation in the octahedral sheets and A can be Ga, Fe, or Mn.[9−11] Two versions of this hexagonal MAO_3 structure exist (Figure 1a,b). The simpler centric structure has a space group of $P6_3/mmc$ with $Z = 2$. The ferroelectric distortion of this structure is unusual in that there is no involvement of empty d orbitals.[12] We now have a space group of $P6_3cm$; the *a* cell edge is increased by $\sqrt{3}$, and *Z* has become 6. Although the coordination of the M cation is trigonal antiprismatic in the centric structure, in the ferroelectric structure, a seventh O

Special Issue: To Honor the Memory of Prof. John D. Corbett

Received: August 20, 2014
Published: October 31, 2014

   dx.doi.org/10.1021/ic502027k | Inorg. Chem. 2015, 54, 837−844

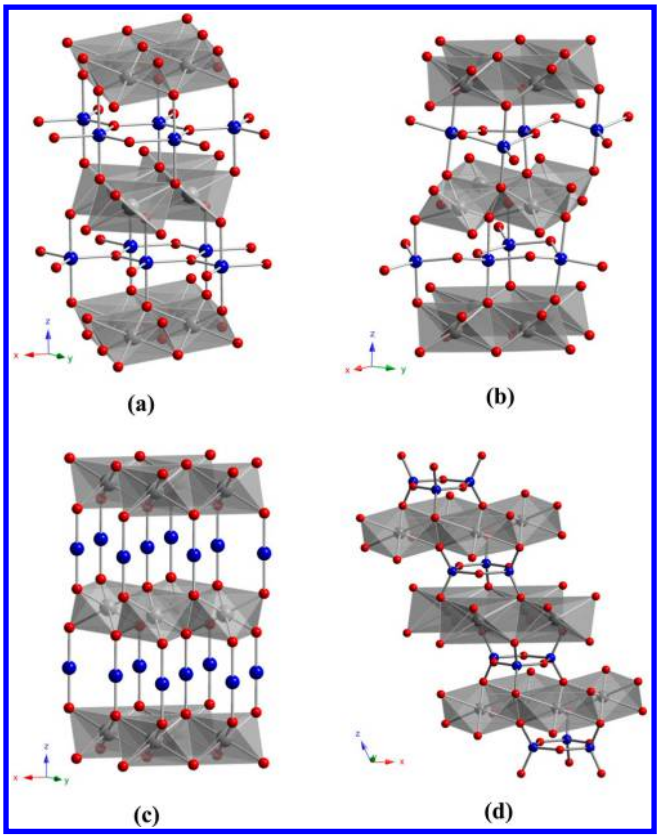

Figure 1. Hexagonal MAO_{2+x} structures based on MO_2 layers. Spheres for M, A, and O are gray, blue, and red, respectively. (a) Hexagonal MAO_3 structure where Ob (basal plane O) atoms are added to the plane of A atoms, which then adopt a TBP coordination. (b) Ferroelectric distortion of MAO_3, where the symmetry remains hexagonal but the unit cell is larger. (c) Delafossite structure for MAO_2 compounds, where A is in 2-fold linear coordination to Oa (apical O) atoms. (d) YBO_3 structure with tetrahedral B (blue) forming B_3O_9 rings.

atom approaches one of the large faces of this trigonal antiprism to the extent that the coordination number (CN) becomes 7 instead of 6. The simple centric structure (Figure 1a) is reported as the room temperature structure for $InGaO_3$, $InFeO_3$, $InMnO_3$, and $RAlO_3$ compounds, where R is a small rare-earth cation.[9−11,13] Subsequently, the ferroelectric structure (Figure 1b) was found as the room temperature structure for $InMnO_3$, as well as for $RInO_3$ and $RGaO_3$ compounds, where R is again a small rare-earth cation.[7,14] The structure for these ferroelectric compounds is reported to become the simple paraelectric structure at temperatures from 500 to 900 °C.[15] The situation for $YFeO_3$ is complex in that ^{57}Fe Mössbauer spectroscopy reveals two types of Fe, suggesting the possibility of the coexistence of paraelectric and ferroelectric forms.[16] Reliable structure determinations exist for all of the above, except for the $RAlO_3$ compounds, which have only been prepared by a citrate route. The only report on the structure of these compounds is from 1963 and is based on powder X-ray diffraction (XRD) data recorded on film.[13] There is no actual structure refinement for any of these hexagonal $RAlO_3$ phases. Our examination of the structure proposed 50 years ago indicates that it is incorrect, and we find that the composition is also incorrect. These hexagonal $RAlO_3$ phases form at 950 °C and convert to the perovskite structure when heated to high temperatures.

It apparently has not been previously recognized that YBO_3 is also a member of the MAO_3 family based on edge-shared MO_2 layers. Early attempts to determine the structure of YBO_3 utilized XRD data. Both powder and single-crystal data indicated a hexagonal unit cell with a = 3.78 Å, c = 8.81 Å, and Z = 2.[17,18] The structure determined was disordered with partially occupied O and B sites. Neutron diffraction studies were impeded by the requirement for the ^{11}B isotope. However, the structure of YBO_3 was recently refined using neutron diffraction data and found to be monoclinic with a = 11.31 Å, b = 6.54 Å, c = 9.55 Å, β = 112.9°, and Z = 12.[19] The coordination of B is tetrahedral with two distinct sites (Figure 1d). The YO_2 sheets of this structure are the same as those in the other MAO_2 and MAO_3 compounds described above.

We recently discovered a brilliant-blue chromophore: Mn^{3+} in TBP coordination in oxides.[20] One example is a composition of the type $YIn_{1-x}Mn_xO_3$ with the hexagonal structure shown in Figure 1b. A primary purpose of this study was to understand why the bright-blue color obtained for $YIn_{1-x}Mn_xO_3$ phases does not occur for $YAl_{1-x}Mn_xO_3$ phases.

EXPERIMENTAL SECTION

The $YAl_{1-x}M_xO_3$ (M = Mn and Fe) and $YB_{1-x}M_xO_3$ (M = Al, Mn, Fe, and Ga) solid solutions were synthesized by a citrate route.[21] Stoichiometric amounts of $Y(NO_3)_3{\cdot}6H_2O$ (Strem Chemicals, 99.9%), $Al(NO_3)_3{\cdot}9H_2O$ (Alfa Aesar, 99.9%), $Mn(NO_3)_2{\cdot}4H_2O$ (Alfa Aesar, 98%), $Fe(NO_3)_3{\cdot}9H_2O$ (Mallinckrodt, AR), H_3BO_3 (Baker Chemical, AR), and $Ga(NO_3)_3{\cdot}8H_2O$ (Strem Chemicals, 99.99%) were dissolved in deionized water (H_3BO_3 in a mixture of deionized water and ethanol before addition). The nitrate solutions were heated with stirring, and the citric acid (Aldrich, 98−102%) was added in a molar ratio of 2:1 citric acid to metal nitrates. The pH of the resulting solutions was then adjusted to 7 using aqueous NH_4OH, and the neutralized solutions were heated until the formation of a dry gel. Dark-brown amorphous powders were obtained after the translucent dry gel was heated at 250 °C for 2 h, and these were then heated at 700−930 °C in air for 10−18 h. To obtain the purest hexagonal "$YAlO_3$" and Al-rich phases, the amorphous powder precursor was placed in a preheated furnace (920 °C) and quenched after heating for 20−30 min. Longer heating time resulted in an increasing amount of an impurity phase like $Y_4Al_2O_9$. The standard solid-state synthesis approach was successful only for the preparation of pure $YMnO_3$, YBO_3, and Al-poor phases.

XRD data were collected on a Rigaku MiniFlex II diffractometer using Cu Kα radiation and a graphite monochromator on the diffracted beam. Data were collected over a 2θ range of 10−120° using a step size of 0.02° with 2 s at each step. Powder neutron diffraction profiles were collected on the 32-counter high-resolution diffractometer BT-1 at the Center for Neutron Research at the National Institute of Standards and Technology. A Cu(311) monochromator, yielding a wavelength of 1.5403(2) Å, was employed. Collimation of 15′ of arc was used before the monochromator, 20′ before the sample, and 7′ before the detectors. The samples (≈10 g) were loaded into V containers of 15.6 mm diameter and 50 mm length. Data were collected at 25, 400, and 800 °C over a 2θ range of 3−167°. XRD and neutron data were refined using the Rietveld method, as implemented in *GSAS-EXPGUI* software.[22] Bond-valence analysis of the neutron structures made use of the bond-valence calculator.[23]

Transmission electron microscopy (TEM) images were obtained on a FEI Titan FEG-TEM instrument operated at 300 kV. TEM samples were ground in isopropyl alcohol and spotted on 300 mesh Cu grids. Solid-state NMR experiments were carried out on a Bruker Avance DSX300 MHz WB NMR spectrometer operating at a field of 7 T. A 4 mm Bruker double-resonance broad-band magic-angle-spinning (MAS) probe was used at a MAS rate of 12 kHz. The IR spectra were recorded in solid phase on a Thermo Scientific Nicolet 6700 Fourier transform infrared spectrometer in the wavelength range

dx.doi.org/10.1021/ic502027k | *Inorg. Chem.* 2015, 54, 837−844

4000−525 cm^{-1}. Thermogravimetric analysis (TGA) data were collected on a TA Instruments SDT-Q600 thermogravimetric analyzer coupled with a Hiden HPR-20 QIC mass spectrometer for simultaneous evolved gas analysis. Data were collected after equilibration at 25 °C, followed by a 20 °C/min ramp up to 1050 °C under an argon atmosphere.

RESULTS AND DISCUSSION

"$YAlO_3$". Figure 2 shows plots of *a*, *c*, *c*/*a*, and volume for the small hexagonal pseudocell (Figure 1a) reported for YAO_3

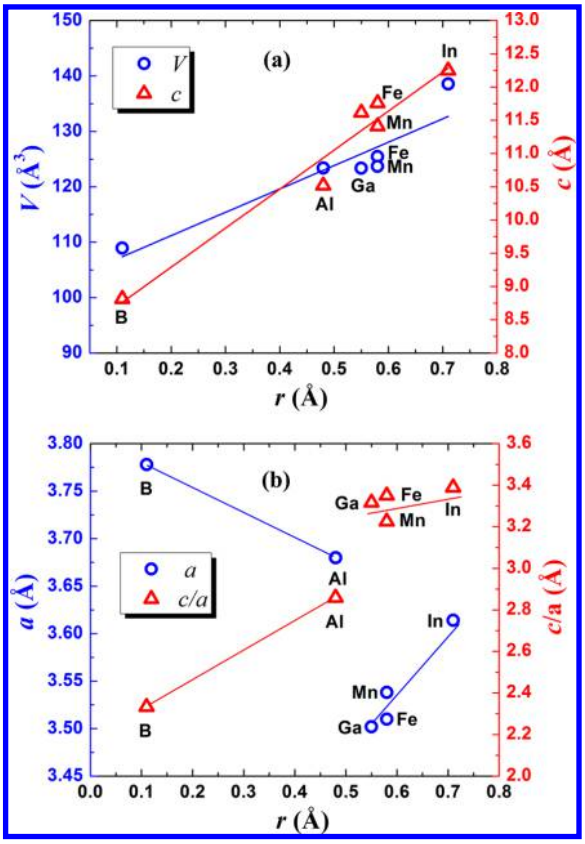

Figure 2. Plots of cell parameters (a) volume *V* and *c* and (b) *a* and *c*/*a* versus the radius of the A cation in hexagonal YAO_3 (A = B, Al, Ga, Mn, Fe, and In). The small hexagonal pseudocell is used. There is no obvious discontinuity in the *V* and *c* plots, but a major discontinuity exists for both *a* and *c*/*a* plots between Ga and Al.[7,13,17,20,21]

compounds, where A = In, Fe, Mn, Ga, Al, and B.[7,13,17,20,21] The coordination of A is tetrahedral when A is B, and it is TBP when A is In, Fe, Mn, and Ga. Assuming that $YAlO_3$ has the same structure as when A is In, Mn, Fe, and Ga, the expected value of *a* for $YAlO_3$ is less than 3.5 Å (Figure 2). The observed value is much higher, even higher than that of $YInO_3$. This is a compelling indication that the structure of hexagonal "$YAlO_3$" is not the same as that for the YAO_3 phases with A = In, Fe, Mn, and Ga.

There is general agreement on the citrate route "$YAlO_3$" values of *a* and *c* based on a simple hexagonal cell. The only variable in this structure is then the *z* parameter of the apical O atom (Oa). As *z* increases, Oa moves away from Y and toward Al, thus increasing the bond-valence sum (BVS) for Al and decreasing the BVS for Y (Figure 3). The reported *z* value[13] of 0.077 gives BVSs of 1.95 for Al and 3.42 for Y, both of which are unreasonable deviations from the expected 3.0 value. Our refined value of *z* based on this model is 0.088. Thus, Oa moves

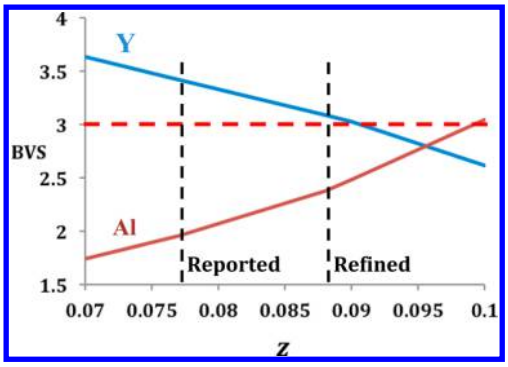

Figure 3. BVSs (solid lines) for Y and Al versus variations in the *z* coordinate of Oa assuming the reported structure.[13] The vertical dashed lines are for the reported and our refined values of *z*. The rest of the *z* values are chosen arbitrarily between 0.07 and 0.1. No value of *z* gives acceptable BVS values (horizontal dashed line) for both Y and Al, but our refined *z* gives the expected BVS value for Y. Our refinement based on $Y_3AlO_8CO_3$ gives BVSs of 2.96 for Al and 2.99 for Y (this work).

away from Y and toward Al, improving the BVS situation. The BVS for Al has increased to 2.37, still unacceptably low. The BVS for Y, however, has deceased to an acceptable 3.09. The BVS for Oa is an acceptable 2.1 for *z* values of 0.077 or 0.088. The BVS for the basal plane O atom (Ob) does not change with variation of *z*, always having a very low value of 1.16. Figure 3 shows that there is no value of *z* that gives acceptable BVS values for Al and Y, indicating that the reported structure cannot be correct, even after refinement. The layer based on Y and Oa appears confirmed with our *z* value of 0.088, but the layer based on Al and Ob must be significantly different from that for the hexagonal structures where A is In, Fe, Mn, or Ga.

Good BVS values for all atoms in the hexagonal $YAlO_3$ can be obtained if the unit cell edges are adjusted. The *a* cell edge must be reduced in order to obtain reasonable Al−Ob distances. The *c* cell edge and *z* can then be adjusted to obtain BVS values of 3 for Y and Al and 2 for both Oa and Ob. The reason this structure is not adopted is apparently the Y−Y repulsion in the edge-shared YO_6 octahedra. This has stretched the structure perpendicular to the *c* axis, causing the BVS values for both Al and Ob to be low.

The behavior of the *a* cell edges in Figure 2 suggests that the structure of $YAlO_3$ might be similar to that of YBO_3. Thus, we considered the possibility that the structure of $YAlO_3$ is related to that of the low-temperature form of YBO_3. This borate structure (Figure 1d) can be generated from the structure with TBP A cations (Figure 1a) by moving both A and Ob atoms off a 3-fold axis toward an adjacent empty 3-fold axis. The tetrahedral borate groups in this structure then form B_3O_9 rings. Hexagonal symmetry is ideally maintained in these B−Ob layers, but the hexagonal symmetry is destroyed by the stacking sequence of the B−Ob layers. The lattice symmetry thus drops to monoclinic. Tetrahedra of Al can also form Al_3O_9 rings, such as, for example, in $Ba_{13}Al_{22}Si_{10}O_{66}$.[24] Furthermore, we find that YBO_3 and "$YAlO_3$" form a complete solid solution (Figure 4), suggesting a strong structural similarity. Thus, we considered that "$YAlO_3$" actually has the low-temperature YBO_3 structure. However, our dynamic light scattering modeling[25] indicates that Al_3O_9 rings are not a good size match for the YO_2 substrate. Also, we observe no peaks in either our XRD or neutron patterns other than those that fit the 3.68 × 10.5 Å hexagonal cell. Our attempts to refine our neutron diffraction

dx.doi.org/10.1021/ic502027k | Inorg. Chem. 2015, 54, 837−844

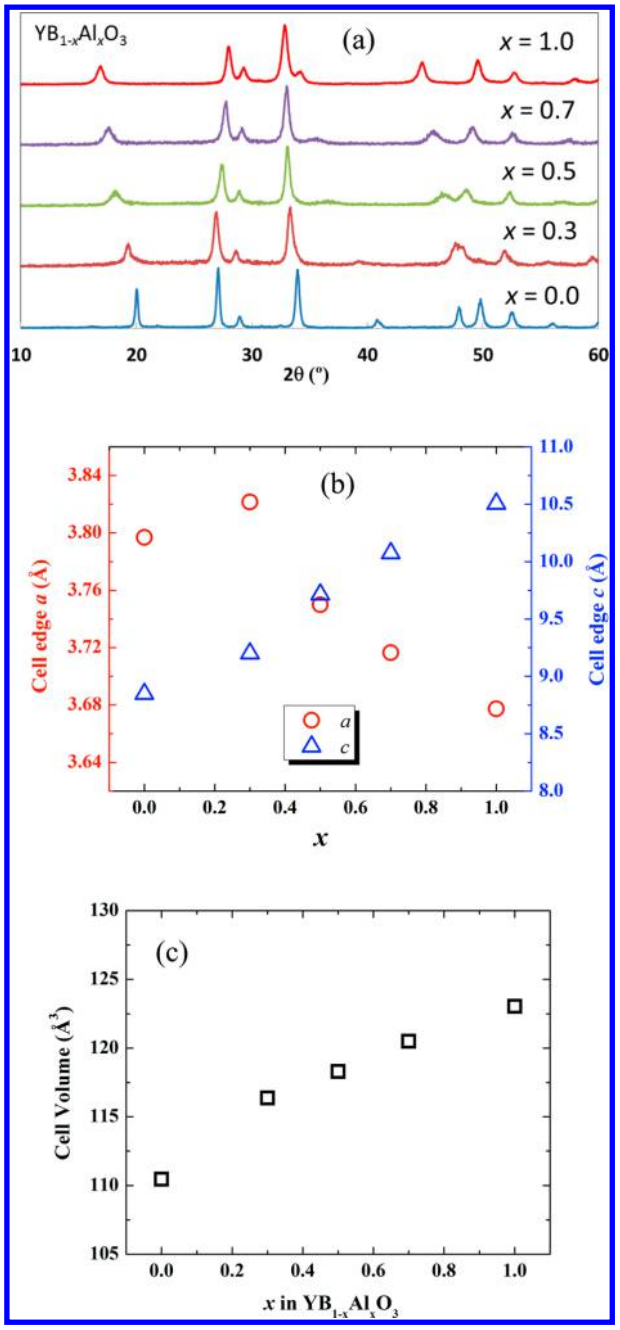

Figure 4. Powder XRD patterns (a) and cell edges versus x (b and c) of the $YB_{1-x}Al_xO_3$ solid solution (x = 0–1) (this work). Estimated uncertainties are smaller than the plotted point size.

data based on the YBO_3 structure failed to give a good fit to our diffraction pattern. Finally, our ^{27}Al NMR data eliminated the YBO_3 structure as a possibility.

It is generally accepted that MAS ^{27}Al NMR provides a reliable indication of the CN of Al in oxides. The accepted chemical shift (δ) ranges in ppm relative to $[Al(H_2O)_6]^{3-}$ are −7 to +16 for AlO_6, +26 to +38 for AlO_5, and +51 to +77 for AlO_4.[26] Our MAS ^{27}Al NMR spectrum (Figure 5) is dominated by a peak (δ = +2.46 ppm). This is well inside the range expected for AlO_6 and far removed from the ranges expected for AlO_5 or AlO_4. This means that, in addition to the two apical O atoms, the Al must be coordinated to four, instead of three, O atoms in the basal plane. If one is restricted to a formula of $YAlO_3$, the CN of O in this basal plane must also increase to 4.

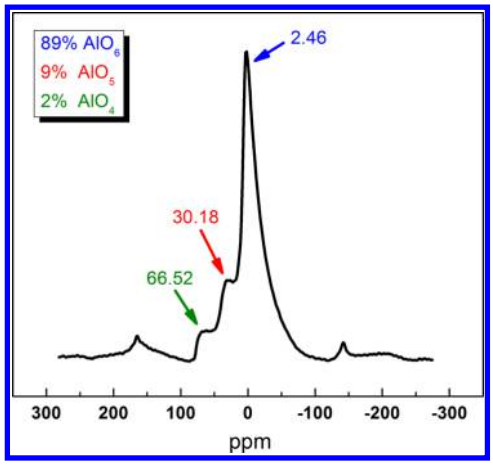

Figure 5. MAS ^{27}Al NMR spectrum showing a major peak (δ = 2.46 ppm) for AlO_6 in a distorted octahedral environment with minor peaks for AlO_5 (δ = 30.2 ppm) and AlO_4 (δ = 66.5 ppm).

A more likely explanation is that the O content has increased above 3 by partial substitution for O^{2-} with CO_3^{2-} groups and/or two OH^- ions. IR spectra showed no apparent evidence of OH^- or H_2O (see Figure S1 in the Supporting Information, SI), and our neutron diffraction data do not show the high background that would occur if significant H were present (see Figure S2 in the SI). Carbonate is detected in our IR spectrum. Our TGA–mass spectrometry results show that, upon transformation to perovskite $YAlO_3$ at about 1050 °C, there is a weight loss and an evolution of CO_2 (see Figure S3 in the SI). Substitution of CO_3^{2-} for O^{2-} in the basal plane can then explain the expansion of the a cell edge (Figure 2) and the increase in the CN of Al to 6, as shown in Figure 6. Because

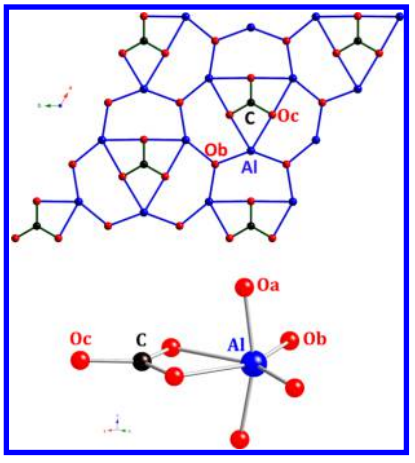

Figure 6. (Top) Structure of the ab plane of $Y_3Al_3O_8CO_3$ with Al, Ob, and CO_3: Al (blue), O (red), and C (black). Carbonate groups have replaced one-third of the Ob atoms, increasing the CN of Al atoms to 6. (Bottom) Coordination of Al: Oa, apical O; Ob, basal plane O; Oc, O connected to C.

one CO_3^{2-} group increases the CN of three Al atoms from 5 to 6, only one-third of the Ob atoms need to be replaced by CO_3^{2-} groups to increase the CN of all of the Al atoms to 6. Thus, the formula for "hexagonal $YAlO_3$" becomes $Y_3Al_3O_8CO_3$ if all Al atoms have a CN of 6. It is important to recall that this compound has never been prepared by the direct reaction of Y and Al oxides or hydroxides.[13,27] The citrate route always used incorporates an organic compound that will oxidize, producing

dx.doi.org/10.1021/ic502027k | Inorg. Chem. 2015, 54, 837–844

CO_2 as it is heated in air. Hereafter, in this paper it will be understood that when hexagonal MAO_3 compounds are referred to, some O atoms may be replaced by CO_3^{2-}. The actual amount of such a carbonate will not always be well determined, but it will not exceed one-ninth of the O atoms.

Samples of $Y_3Al_3O_8CO_3$ ("hexagonal $YAlO_3$", hereafter referred to as $Y_3Al_3O_8CO_3$ unless otherwise specified) are poorly crystalline and are never completely phase pure. All diffraction patterns of $Y_3Al_3O_8CO_3$ obtained by us and reported by others[27] have broad peaks indicative of a crystallite size of about 20 nm. Weak peaks of $Y_4Al_2O_9$ are present. Attempts to improve the crystallinity and phase purity using long heating times or higher temperatures lead to some decomposition of the hexagonal phase. TEM shows many crystallites smaller than 20 nm and some amorphous regions (see Figure S4 in the SI). Superstructure peaks based on complete ordering of the CO_3^{2-} groups, as shown in Figure 6, do not appear in our powder neutron or XRD patterns. These superstructure peaks would be too weak to observe in XRD patterns, but in the neutron pattern, superstructure peaks at 2θ = 16.05 and 23.41° would have intensities comparable to the weakest peaks actually observed. Furthermore, we find no evidence of a superstructure in our TEM studies (see Figure S4 in the SI). Thus, we assume that Figure 6 represents an ideal structure and that the actual structure is disordered in some manner. Rietveld refinements (Table 1) were therefore based on the cell in space group $P6_3/mmc$ in Figure 1a. Refinement of the C replacement for Ob gave one-third C and two-thirds O on this site, confirming the expectation based in Figure 6 where one-third of Ob is replaced by CO_3. This brings the CN of Al up to 6. Difference Fourier maps from our neutron diffraction data indicated nuclear density at the sites expected for the O atoms of carbonate groups substituting for Ob. It was also evident that Al was displaced from the 3-fold axis away from the carbonate group. Refinement results are given in Table 1, and Rietveld fits are shown in Figures 7 and S5 in the SI. The fit based on the reported structure shows a poor fit, and refining this model results in only minor improvement. Our refined model with carbonate dramatically improves the fit. This structure for $Y_3AlO_8CO_3$ gives BVS values of 2.99 for Y, 2.96 for Al, and 2.13 for Oa. The BVS for Ob has increased from 1.16 to 1.57 in this model, improved but still low. It is a characteristic of the hexagonal MAO_3 compounds with TBP A cations that Ob is significantly underbonded, which gives rise to a ferroelectric distortion.[12] The high U values for Ob and Oc (Table 1) suggest that this same type of distortion is likely present in $Y_3Al_3O_8CO_3$ but in a disordered manner. A poorly defined peak at a very low angle (2θ = ~7.5°) was always observed in both our neutron and XRD patterns (Figure S6 in the SI). We cannot attribute this peak to an impurity phase, and it does not occur in the XRD patterns of other "$RAlO_3$" phases.

Table 1. Summary of $Y_3Al_3O_8CO_3$ Structure Refinement[a]

	25 °C	800 °C
a, Å	3.6798(1)	3.7076(1)
c, Å	10.496(1)	10.552(1)
z(Oa)	0.0893(2)	0.0925(3)
x(Al)	0.375(4)	0.382(2)
x(Oc)	0.420(4)	0.413(4)
Al−Oa (×2), Å	1.707(5)	1.691(4)
Al−Ob (×2), Å	2.01(1)	2.003(6)
Al−Oc (×2), Å	2.07(2)	2.13(1)
Al−O average, Å	1.93(1)	1.94(1)
C−Oc (×3), Å	1.32(2)	1.33(2)
Y−Oa (×6), Å	2.322(1)	2.353(1)
Al displacement[b], Å	0.26(2)	0.31(2)
Ob:C ratio	0.67:0.33(1)	0.66:0.34(1)
Y: U_{iso}, Å[b]	0.035(1)	0.0522(4)
Al: U_{iso}, Å[b]	0.073(2)	0.068(2)
C: U_{iso}, Å[b]	0.051(2)	0.061(2)
Oa: U_{iso}, Å[b]	0.038(1)	0.063(2)
Ob: U_{iso}, Å[b]	0.30(1)	0.43(1)
Oc: U_{iso}, Å[b]	0.35(1)	0.33(1)

[a]Space group: $P6_3/mmc$. Y: 2a, (0, 0, 0). Al: 6h, (x, $2x$, $^1/_4$). Oa: 4f, ($^1/_3$, $^2/_3$, z). Ob and C: 2b, (0, 0, $^1/_4$). Oc: 6h, ($2x$, x, $^1/_4$). Oa: apical O. Ob: basal plane O. Oc: O connected to C. Standard uncertainties, given in parentheses, do not reflect the uncertainty in the neutron wavelength. [b]Displacement of Al from the 3-fold axis. [c]Anisotropic U values are given in the CIF file.

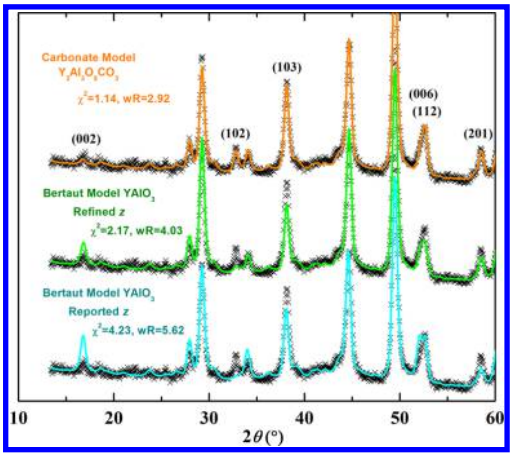

Figure 7. Rietveld fits of neutron diffraction data. The fit for $Y_3Al_3O_8CO_3$ is shown to be 167° in Figure S5 in the SI.

The ^{27}Al NMR spectrum (Figure 5) also shows small peaks due to AlO_5 and AlO_4. The peak with a chemical shift of 66.5 ppm indicating AlO_4 is presumably from the $Y_4Al_2O_9$ impurity detected in our neutron diffraction patterns (see Figure S5 in the SI). The peak with a chemical shift of 30.2 ppm indicating AlO_5 could arise from an amorphous impurity (see Figure S4 in the SI). MAS ^{27}Al NMR studies of Al-rich glasses in the Al_2O_3−Y_2O_3 system have shown high concentrations (~40%) of AlO_5.[28] However, it is likely that this peak is due, at least in part, to the main $Y_3Al_3O_8CO_3$ phase reformulated as $Y_3Al_3O_{9-x}(CO_3)_x$, where x may be slightly less than 1.0. Refinements of the C content and the associated O content for a carbonate group do not suggest that x is less than 1.0 (Table 1). However, if we were to assume that all of AlO_5 shown by NMR arises from the oxycarbonate phase, a formula of $Y_3Al_3O_{8.08}(CO_3)_{0.92}$ could account for the relative amounts of AlO_6 and AlO_5 indicated by our ^{27}Al NMR data. If a very small number of carbonate groups were missing from the $Y_3Al_3O_8CO_3$ structure (Figure 6a) and replaced by O^{2-}, clusters of three Al atoms in TBP coordination would be produced, and the superstructure peaks anticipated from Figure 6a would be slightly weakened but would still be present. Another possibility is that the TBP Al atoms would occur isolated from other TBP Al atoms as a point defect depicted in Figure S7 in the SI. This would destroy the periodicity of the

dx.doi.org/10.1021/ic502027k | Inorg. Chem. 2015, 54, 837−844

CO_3^{2-} groups, as shown in Figure 6a; thus, there would be no superstructure consistent with our observations.

It is unusual to form an oxycarbonate on preparing oxides in air, even with CO_2 produced during the synthesis of a precursor containing organics. However, carbonates such as $BaCO_3$ and $SrCO_3$ are stable to high temperature, and ternary oxides of Cu and Mn are known to form oxycarbonates upon heating in air if they also contain Ba or Sr.[29,30] In these cases, the carbonate group is bound directly to Ba or Sr, and Cu or Mn forms only one bond to the carbonate group. A unique feature of $Y_3Al_3O_8CO_3$ is that each Al atom forms two bonds to one carbonate group. Although Y is a basic cation, it is considerably less basic than Ba or Sr. Decomposition of $Y_2O_2CO_3$ occurs at about 500 °C.[31]

Related Phases. The behavior of the unit cell edges for the $YB_{1-x}Al_xO_3$ solid solution (Figure 4) suggests that Al initially substitutes for B in the B_3O_9 rings of the YBO_3 structure and that this results in an increase in both *a* and *c* due to the larger size of Al relative to B. It would appear that the limit of this substitution might be one Al atom per ring ($x = {}^1/_3$). Additional Al then presumably has an environment similar to that in $Y_3Al_3O_8CO_3$, and this causes a decrease in *a* with an increase in the Al concentration even though Al is larger than B. Further B and Al NMR studies are underway to evaluate this model. A qualitative indication of the carbonate content by IR spectra as a function of the B content is impeded by borate absorption in the same region as carbonate. We find that YBO_3 also forms solid solutions with hexagonal $YFeO_3$, $YMnO_3$, and $YGaO_3$; details are given in Figure S8 in the SI.

A complete $YAl_{1-x}Mn_xO_3$ solid solution can be prepared by the citrate route (see Figure S9 in the SI), and Mn-rich phases can be prepared by heating binary oxide mixtures in air. The variations of *a*, *c*, and *V* with *x* are essentially linear (Figure 8), suggesting a gradual decrease of carbonate with increasing *x*. The superstructure reflections in $YMnO_3$ due to the ferroelectric distortion remain present at $x = 0.9$ but have disappeared for lower values of *x* (see Figure S9 in the SI). The disorder associated with the Al substitution for Mn has disrupted the long-range forces required for the transition to the ferroelectric state. Although a blue color develops with Mn substitution, it is a dark navy blue rather than the brilliant-blue color observed for $YIn_{1-x}Mn_xO_3$ phases. The colors and diffuse-reflectance spectra for $YAl_{1-x}Mn_xO_3$ phases are shown in Figure S9 in the SI. The absence of bright color is presumably due to the destruction of TBP sites caused by carbonate substitution (see Figure S10 in the SI). A significant fraction of Mn^{3+} will be on the highly distorted octahedral site, which produces color, but not the bright-blue color associated with the TBP site.

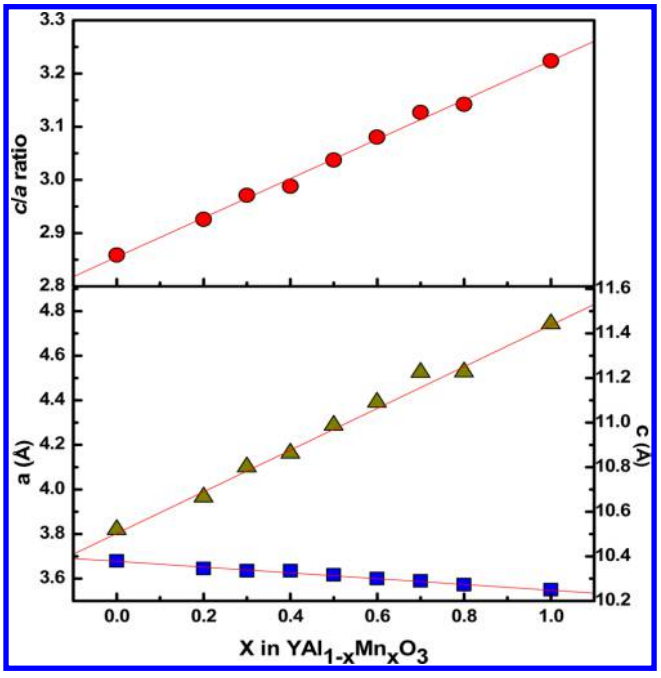

Figure 8. Cell edges versus *x* for $YAl_{1-x}Mn_xO_3$ phases. Estimated uncertainties are smaller than the plotted point size.

The synthesis of $YGaO_3$ has been reported at very high temperature (>1950 °C) or by a citrate route at much lower temperatures (~850 °C).[7,8] The unit cell dimensions of our product prepared by the citrate route are $a = 6.135$ Å and $c = 11.57$ Å. These are significantly different from those reported ($a = 6.065$ Å and $c = 11.615$ Å) for a crystal prepared at high temperature.[7] (see Figure S11a in the SI). This suggests that an increase in the *a* and *b* cell edges is due to carbonate substitution as occurs in $Y_3Al_3O_{9-x}(CO_3)_x$. The small decrease in the *c* cell edge upon carbonate incorporation is expected because stretching the YO_2 layer in the *ab* plane will cause this layer to shrink in the *c* direction. The presence of carbonate in citrate-prepared $Y_3Ga_3O_{9-x}(CO_3)_x$ was confirmed by IR data (see Figure S1 in the SI). Expansion of the *a* cell edge is much more pronounced in the citrate-prepared hexagonal "$RGaO_3$" phases where R is La, Pr, Nd, Sm, or Eu (see Figure S11b,c in the SI).[6] This suggests a carbonate concentration much higher here than that for the citrate-prepared phase with R = Y.

Phases of the type $YAl_{1-x}Fe_xO_3$ could only be prepared through the citrate route (see Figure S12 in the SI), and lattice constants as a function of *x* are shown in Figure 9. Unlike the $YAl_{1-x}Mn_xO_3$ solid solution, there is now a miscibility gap and the variation of *a* and *c* with *x* deviates strongly from linear. It would appear that for $YAl_{1-x}Fe_xO_3$ the carbonate level remains high upon the initial substitution of Fe up to the miscibility gap. Then there is an abrupt decrease in the carbonate concentration of the Fe-rich side of the gap, and this leads to the abrupt decrease in the *a* cell edge and unit cell volume. This explanation is qualitatively supported by the carbonate IR results (see Figure S1 in the SI). Some carbonate is always present in hexagonal $YFeO_3$ itself. This carbonate substitution is apparently related to the second Fe site found by ^{57}Fe Mössbauer spectroscopy.[15,32] We find that our ^{57}Fe Mössbauer spectrum for hexagonal $YFeO_3$ can be well fit based on 89% Fe^{3+} in CN 5 and 11% Fe^{3+} in CN 6. Because each carbonate group would convert three Fe sites to CN 6, this would give a formula $Y_3Fe_3O_{8.96}(CO_3)_{0.04}$. Further ^{57}Fe Mössbauer analysis of various samples of hexagonal $YFeO_3$ and its solid solutions is underway. The colors and diffuse-reflectance spectra for the $YAl_{1-x}Fe_xO_3$ phases are shown in Figure S12b,c in the SI.

CONCLUSIONS

Our studies indicate that the structure for $Y_3Al_3O_8CO_3$ shown in Figure 6 is basically correct for one layer. However, it appears that an occasional carbonate group may be missing, and this site is then occupied by just one O atom, maintaining charge balance but decreasing the CN of three neighboring Al atoms from 6 to 5, as suggested by our NMR results. This defect (see Figure S7 in the SI) would produce disorder within a layer and be a factor in preventing an ordered stacking of the layers

dx.doi.org/10.1021/ic502027k | Inorg. Chem. 2015, 54, 837−844

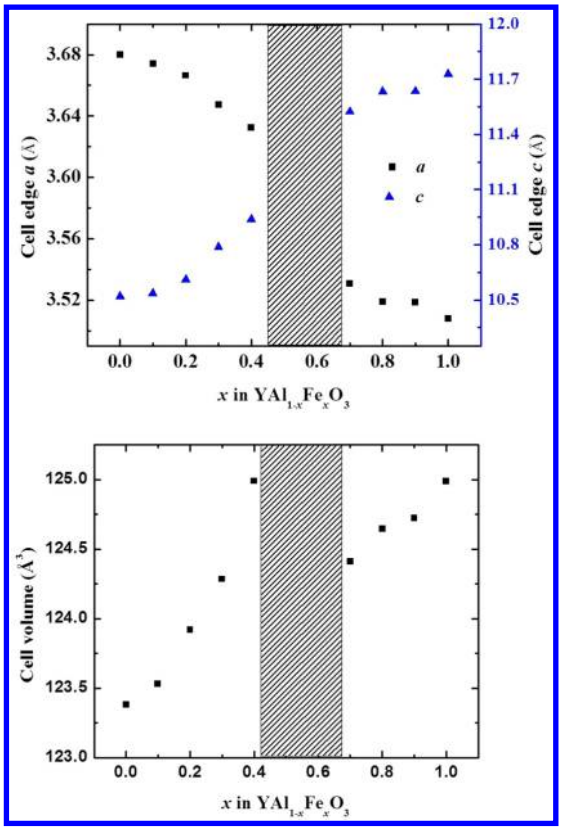

Figure 9. Cell edges versus x for $YAl_{1-x}Fe_xO_3$ phases. Estimated uncertainties are smaller than the plotted point size.

shown in Figure 6. A structure well ordered in three dimensions would result in a superstructure that should be apparent in our neutron diffraction and TEM results. We find no evidence for such a superstructure. Disorder is also evident in high displacement factors for Ob and Oc. This disorder is likely a factor in allowing solid solutions of $Y_3Al_3O_8CO_3$ to form with YBO_3 and $YMnO_3$. The YO_2 layers connected by A cations form the backbone of these structures. The A cations can have a disordered mixture of CNs ranging from 4 to 5 to 6 in these solid solutions with a variable amount of carbonate present.

There is always a problem with the ideal hexagonal MAO_3 structure from the point of view of BVS values. The M−M repulsion across edges of the edge-shared MO_6 octahedra resists contraction of the a and b cell edges as A becomes smaller. This causes the A−Ob distances to become stretched relative to their optimum values. In the YAO_3 series, the problem is not serious when A is In, where the BVS values for In and Ob are 2.92 and 1.83, respectively, in the ideal structure (Figure 1a). The ferroelectric distortion that occurs in $YInO_3$ does not increase the BVS for In, but it increases the BVS for Ob to 1.94 and it reduces the repulsion between Y^{3+} cations because they now are not all at the same z value along the c axis. The BVS situation becomes worse upon reduction of the A cation size to that of Fe^{3+}. Now the BVS values for Fe and Ob have dropped to 2.62 and 1.62, respectively.[21] Further reduction of the size of A to that of Al gives BVS values of 2.37 and 1.16 for A and Ob, respectively. For $Y_3Al_3O_8CO_3$, the replacement of one-third of Ob with CO_3 groups brings the BVS for Al up to 3.0, and the displacement of Al toward the remaining Ob atoms brings their BVS value from 1.1 up to 1.6. For all of these hexagonal MAO_3 compounds, a ferroelectric-type distortion will increase the BVS for Ob. In principle, the BVS problem for A and Ob could be eliminated without ferroelectric distortion by simply reducing the length of the a and b cell edges, thus decreasing the A−Ob distances. Assuming no change in the observed A−Oa distance, the changes of a and b in the ideal structure (Figure 1) required to bring the BVS of A up to 3.0 are 3.66 → 3.63 for In, 3.50 → 3.36 for Fe, 3.51→ 3.43 for Ga, and 3.68 →3.30 for Al. This change in a and b would bring the BVS values for Ob up to 1.91 (In), 2.02 (Fe), 1.7 (Ga), and 1.78 (Al). However, this shrinkage is prevented by Y−Y repulsion. Hexagonal $YMnO_3$ presents a special case. Because of orbital ordering for Mn^{3+} in TBP coordination, the Mn−Oa bonds are much shorter than the Mn−Ob bonds. Consequently, the c cell edge in $YMnO_3$ is much shorter than that in $YFeO_3$ (Figure 2) even though Fe^{3+} and Mn^{3+} have the same radii. The Mn and Ob BVS values for the ideal structure are 2.85 and 1.52, respectively. Decreasing a from 3.56 to 3.50 would bring the BVS of Mn up to 3.0 and the BVS of Ob up to 1.67. The ferroelectric distortion that occurs for $YMnO_3$ does not impact the 2.85 BVS for Mn, but it brings the BVS for Ob up to 2.0.

■ ASSOCIATED CONTENT

Supporting Information

Figures S1−S12 and X-ray crystallographic data in CIF format. This material is available free of charge via the Internet at http://pubs.acs.org.

■ AUTHOR INFORMATION

Corresponding Author

*E-mail: mas.subramanian@oregonstate.edu.

Notes

The authors declare no competing financial interest.

■ ACKNOWLEDGMENTS

This work was supported by NSF Grant DMR 0804167. We thank Dr. Jerry Hu for solid-state NMR measurements and acknowledge use of the facilities of the UCSB Materials Research Laboratory. We acknowledge support of the National Institute of Standards and Technology, U.S. Department of Commerce, in providing the neutron research facilities used in this work. The identification of any commercial product or tradename does not imply endorsement or recommendation by the National Institute of Standards and Technology.

■ REFERENCES

(1) Berthelot, R.; Schmidt, W.; Muir, S.; Eilertsen, J.; Etienne, L.; Sleight, A. W.; Subramanian, M. A. *Inorg. Chem.* **2012**, *51*, 5377.
(2) Paulson, J. M.; Donaberger, R. A.; Dahn, J. R. *Chem. Mater.* **2000**, *12*, 2257−2267.
(3) Delmas, C.; Braconnier, J. J.; Hagenmuller, P. *Mater. Res. Bull.* **1982**, *17*, 117.
(4) Li, J.; Yokochi, A.; Sleight, A. W. *Solid State Sci.* **2004**, *6*, 831−839.
(5) Jiang, P.; Berthelot, R.; Li, J.; Sleight, A. W.; Subramanian, M. A. *Mater. Res. Bull.* **2013**, *48*, 2237−2239.
(6) Sallavuard, G.; Szabo, G.; Paris, R. A. *C. R. Hebd. Seances Acad. Sci.* **1969**, *268C*, 1050−1053.
(7) Geller, S.; Jeffries, J. B.; Curlander, P. J. *Acta Crystallogr.* **1975**, *B31*, 2770−2774.
(8) Tamilarasan, S.; Sarma, D.; Reddy, M. L. P.; Natarajan, S.; Gopalakrishnan, J. *RSC Adv.* **2013**, *3*, 3199−3202.
(9) Shannon, R. D. *Acta Crystallogr.* **1976**, *A32*, 751−767.
(10) Giaquinta, D. M.; zur Loye, H. C. *J. Am. Chem. Soc.* **1992**, *114*, 10952−10953.

(11) Giaquinta, D. M.; Davis, W. M.; zur Loye, H. C. *Acta Crystallogr.* **1994**, *C50*, 5−7.
(12) Sleight, A. W. *Prog. Solid State Chem.* **2009**, *37*, 251−261.
(13) Bertaut, F.; Mareschal, J. *C. R. Hebd. Seances Acad. Sci.* **1963**, *257*, 867−870.
(14) Greedan, J. E.; Bieringer, M.; Britten, J. F.; Giaquinta, D. M.; zur Loye, H.-C. *J. Solid State Chem.* **1995**, *116*, 118−130.
(15) Abrahams, S. C. *Acta Crystallogr.* **2001**, *B57*, 485−490.
(16) Jiang, P.; Li, J.; Sleight, A. W.; Subramanian, M. A. *Inorg. Chem.* **2011**, *50*, 5858−5860.
(17) Newnham, R. E.; Redman, M. J.; Santoro, R. P. *J. Am. Ceram. Soc.* **1963**, *46*, 253−256.
(18) Chadeyron, G.; El-Ghozzi, M.; Mahiou, R.; Arbus, A.; Cousseins, J. C. *J. Solid State Chem.* **1997**, *128*, 261−266.
(19) Lin, J.; Sheptyakov, D.; Wang, Y.; Allenspach, P. *Chem. Mater.* **2004**, *16*, 2418−2424.
(20) Smith, A. E.; Mizoguchi, H.; Delaney, K.; Spaldin, N. A.; Sleight, A. W.; Subramanian, M. A. *J. Am. Chem. Soc.* **2009**, *131*, 17084−17086.
(21) Li, J.; Singh, U. G.; Schladt, T. D.; Stalick, J. K.; Scott, S. L.; Seshadri, R. *Chem. Mater.* **2008**, *20*, 6567−6576.
(22) (a) Larson, A. C.; Von Dreele, R. B. *General Structure Analysis System (GSAS)*; Report LAUR 86-748; Los Alamos National Laboratory: Los Almos, NM, 1994. (b) Toby, B. H. *J. Appl. Crystallogr.* **2001**, *34*, 210−213.
(23) Hormillosa, C.; Healy, S.; Stephen, T.; Brown, I. D. *Bond Valence Calculator*, version 2.0, 1993; http://ccp14.ac.uk (date accessed: 04/09/2014).
(24) Gebert, W. *Z. Kristallogr.* **1972**, *135*, 437−452.
(25) Meier, W. M.; Villiger, H. *Z. Kristallogr.* **1996**, *129*, 161.
(26) Smith, M. E. *Appl. Magn. Reson.* **1993**, *4*, 1−64.
(27) Lu, W.; Ma, X.; Zhou, H.; Chen, G.; Li, J.; Zhu, Z.; You, Z.; Tu, C. *J. Phys. Chem. C* **2008**, *112*, 15071−15074.
(28) Florian, P.; Gervais, M.; Douy, A.; Massiot, D.; Courtures, J.-P. *J. Phys. Chem. B* **2001**, *105*, 379−391.
(29) Creaves, C.; Slater, P. R. *Physica C* **1991**, *175*, 172−178.
(30) Caignaert, V.; Domenges, B.; Raveau, B. *J. Solid State Chem.* **1995**, *120*, 279−289.
(31) Imanaka, N.; Masui, T.; Mayama, Y.; Koyabu, K. *J. Solid State Chem.* **2005**, *178*, 3601−3603.
(32) Downie, L. J.; Goff, R. J.; Kockelmann, W.; Forder, S. D.; Parker, J. E.; Morrison, F. D.; Lightfoot, P. *J. Solid State Chem.* **2012**, *190*, 52−60.